Characterizing sea state variability along the French Atlantic coast

Grégoire MUREAU [1], Guillaume DODET [2] Serge SUANEZ [3]

1. Ifremer, Infrastructures de Recherche et Systèmes d'Information (IRSI), Service Ingénierie des Systèmes d'Information, Brest, France.
   gregoire.mureau@ifremer.fr
2. Université de Brest, CNRS, Ifremer, IRD, Laboratoire d'Océanographie Physique et Spatiale, Brest, France.
   guillaume.dodet@ifremer.fr
3. Université de Brest, CNRS, UMR 6554 Littoral, Environnement, Géomatique, Télédétection, Institut Universitaire Européen de la Mer, Brest, France.

Abstract :

Sea states condition a large part of marine activities in the coastal zone, such as navigation, fishing, maritime engineering, port logistics, and even nautical leisure activities. In order to monitor, understand and predict sea states, it is essential to have access to observation databases both in the form of historical archives and near real time data. These data generally come from networks of in situ measuring instruments, coastal radars, satellite remote sensing or modeling systems, each of which has its strengths and limitations. In France, the *Centre d'Archivage National des Données de Houle In Situ* (CANDHIS) aims to disseminate wave buoy data acquired in the coastal zone to the scientific community, maritime professionals and the general public. The CANDHIS network includes around a hundred wave recorders deployed along the French coasts and overseas. These instruments are mostly located within 50 kilometers from the coast and provide every hour sea state parameters, such as the significant wave height, wave period and wave direction. However, depending on the environmental characteristics of the sites (bathymetry, currents, climatology) selected to deploy the instruments, the spatial representativeness of these acquisitions can vary significantly. In this study, we seek to characterize the scales of spatial representativeness of the sea state parameters recorded by 11 buoys of the CANDHIS network along the French Atlantic coastline from retrospective simulations obtained using a high-resolution regional spectral wave model. For each of the stations, areas of representativeness are defined from the degree of similarity between the time series simulated at the station and those of neighboring nodes, estimated from statistical parameters. The variability and spatial distribution of the representativeness areas obtained for all of the stations along the coast of mainland France are then analyzed with regard to the very diverse environmental conditions encountered along this coast. The consequences for the exploitation of these data are finally discussed.

Thème 1 – Hydrodynamique marine et côtière

Keywords:
Sea states, Wave buoys, In situ observations, Numerical modelling.

1. Introduction

Sea state information in the coastal zone is key for many activities, including navigation safety, fishing, marine engineering, port logistics, and nautical leisure activities. There are many techniques to measure sea states, either from in situ instruments (e.g. wave buoys, pressure transducers) or remote instruments (e.g. radar altimeters, lidars, video cameras), each of them presenting specific advantages, limitations and requirements (ARDHUIN *et al.*, 2019). For instance, wave buoys can provide sea state parameters with good accuracy over long periods of times at hourly resolution, but they only provide local information and are blind to any neighbor changes in the wave field. On the contrary, satellite-borne altimeters are able to measure the significant wave height along their tracks over the globe, but only with a few-day revisit time period, and with degraded performance near the coast (VIGNUDELLI *et al.*, 2019). Given the numerous physical processes that affect wave propagation and transformation in the coastal zone, where strong current and bathymetric gradients interact with the incident wave field, it is particularly necessary to characterize coastal sea state variability from existing observations and numerical models. With the goal to perform robust comparisons between the radar altimeter on board the Sentinel-3 mission and wave buoys deployed along the UK coastline, NENCIOLI & QUARTLY (2019) developed a methodology to estimate correlation areas for the significant wave height around the wave buoys using a numerical wave model hindcast. In this study, we apply a similar methodology to a set of 11 wave buoys along the French Atlantic coasts, using an unstructured high-resolution wave model and with revisited error thresholds. In addition, we apply the methodology to the peak period and peak direction in order to get a broader view of sea state variability. Our results show very diverse and constrained patterns of variability that illustrate the complexity of wave transformations in coastal areas.

2. Methods and datasets

2.1 In situ observations

The in-situ wave observations used for this study are from the CANDHIS network, the French National Archiving Center for In Situ Wave Data (*Centre d'Archivage National des Données de Houle In Situ*), which is managed by the *Centre d'Études et d'expertise sur les Risques, l'Environnement, la Mobilité et l'Aménagement* (CEREMA). A set of 11 wave buoys located along the French Atlantic coast were selected (figure 1). Only buoys deployed over a minimum period of one year and located more than 2 km off the coast were selected. These buoys are all located within less than 20km from the coast and in depths between 10-70m (table 1).
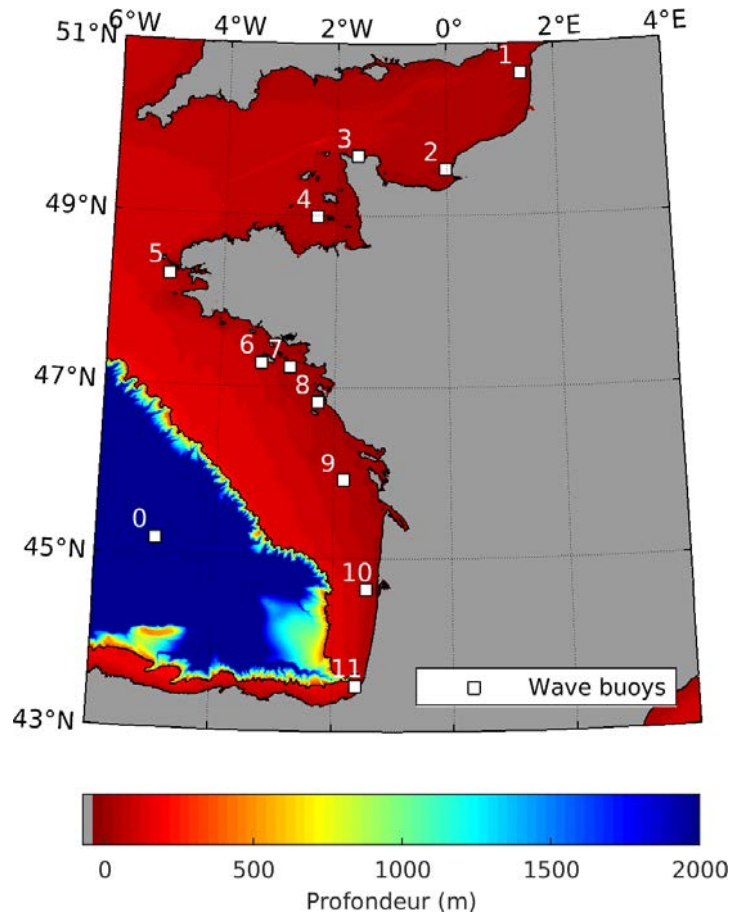
Figure 1. Map of selected in situ wave buoys along the French Atlantic coast.

Table 1. List of wave buoys selected to investigate sea state variability along the French Atlantic coast.

ID	Platform code	Lon. (°)	Lat. (°)	Depth (m)	Distance to the coast (km)	Distance to the nearest model node (km)
0	6200001	-5.000	45.200	4652.9	183.74	4.74
1	62072	1.370	50.659	38.1	13.90	1.01
2	62076	-0.034	49.544	17.0	17.53	0.06
3	6200059	-1.620	49.695	26.0	2.3	0.33
4	62077	-2.343	48.988	35.3	12.30	0.71
5	6200069	-4.968	48.290	64.9	6.13	0.41
5	6200074	-3.285	47.285	50.2	3.80	0.25
7	6200078	-2.787	47.239	34.0	9.64	0.27
8	6200067	-2.292	46.833	10.5	12.17	0.05
9	6200080	-1.834	45.916	50.9	34.5	1.33
10	6200064	-1.447	44.651	51.2	16.39	0.56
11	6200066	-1.614	43.530	52.7	5.98	0.47

In addition, the Gascogne buoy (station 6200001), an offshore buoy operated by the UK Met Office located in the Bay of Biscay, was also included to provide a comparison between coastal and offshore stations. For each station, the significant wave height (Hs), the peak period (Tp) and the peak direction (Dp) were downloaded from the portal of the Copernicus Marine Service IN Situ Thematic Assembly Center (CMEMS INSTAC, http://www.marineinsitu.eu/). Only quality controlled records were analyzed. Note that for some of the stations, only Hs was available.

2.2 <u>Wave model hindcast</u>

The wave model hindcast used in this study is being developed at IFREMER in the context of the ResourceCODE project (OCEAN ERA-Net cofound) with the aim to provide accurate long-term sea state information for the exploitation of Marine Renewable Energy (https://resourcecode.ifremer.fr/). It is a regional implementation of the WAVEWATCH III □ (hereafter WW3) spectral wave model on a high-resolution unstructured mesh extending from the south of Spain to the Faroe Islands, and from the western Irish continental shelf to the Baltic Sea (-12°W to 13.5°E, 36°N to 63°N). The hindcast covers a 28-year period, from 1993 to 2020. The bathymetry combines data from the EMODnet dataset (EMODnet 2016) and the HOMONIM dataset provided by the French Naval Hydrographic and Oceanographic Service (Shom) with a 0.001° resolution over the Channel and the Bay of Biscay. The spatial mesh contains 328,000 nodes and the resolution ranges from 10 km offshore to 200 m near the coast. The spectral grid consists of 36 directions and 36 exponentially spaced frequencies, from 0.0339Hz to 0.9526Hz. The physical parameterization corresponds to test T475, as described in ALDAY *et al.,* (2021), which uses adjusted parameters for the wind-wave generation and swell dumping terms. The model is forced along its boundaries with wave spectra generated by a global WW3 wave model hindcast forced with ERA-5 hourly wind fields (HERSBACH *et al.,* 2020) and CMEMS-Globcurrent surface current fields (Global Ocean Multi Observation Product, MULTIOBS_GLO_PHY_REP_015_004). The regional model is forced by ERA-5 wind fields (with a bias correction for wind speeds larger than 21m/s), and with currents and water levels reconstructed from the MARS2D and FES2014 tidal harmonics database. Detailed information on the ResourceCODE marine data toolbox implementation and validation can be found in ACCENSI *et al.*, (2021) and ALDAY *et al.*, (2022). Implementation and validation of the global wave hindcast are described in ALDAY *et al.*, (2021).

2.3 <u>Sea state variability characterization</u>

The first step of this study is the validation of the high-resolution wave model hindcast against in situ data, in order to estimate uncertainties in the modeled wave parameters. To perform this validation, hourly model outputs were extracted from the nodes closest to the buoy locations. These distances are between 0.05-5km and largely depends on the

buoy location with respect to the coast since the model mesh resolution decreases shoreward (table 1). The following statistical indicators were computed: bias, normalized bias, root mean square error (RMSE), normalized root mean square error (NRMSE), scatter index (SI), coefficient of determination (R^2). These parameters are estimated as follows:

$$Bias = \frac{1}{N}\sum(X_{Mod} - X_{Obs}) \tag{1}$$

$$RMSE = \sqrt{\frac{1}{N}\sum(X_{Mod} - X_{Obs})^2} \tag{2}$$

$$NRMSE = \sqrt{\frac{\sum(X_{Mod} - X_{Obs})^2}{\sum X_{Obs}^2}} \tag{3}$$

$$SI = \sqrt{\frac{\sum\left((X_{Mod} - \overline{X_{Mod}}) - (X_{Obs} - \overline{X_{Obs}})\right)^2}{\sum X_{Obs}^2}} \tag{4}$$

$$R = \frac{1}{N}\frac{\sum\left((X_{Mod} - \overline{X_{Mod}}) - (X_{Obs} - \overline{X_{Obs}})\right)}{\sigma_{Mod}\sigma_{Obs}} \tag{5}$$

where X_{Mod} and X_{Obs} correspond to Model and in situ data, respectively, and σ_{Mod} and σ_{Obs} correspond to the standard deviation of model and in situ data, respectively.

In a second step, the variability of sea states at each buoy location is investigated based on the model hindcast results. The simulated Hs, Tp and Dp fields are used to identify the area around each buoy where wave characteristics remain similar to those observed at the buoy site. For this purpose, the systematic (bias) and random errors (RMSE, R) are computed between the modeled wave parameters at the buoy location and at every node surrounding the wave buoy within a 100x100 km² area. Note that in the case of our spatial variability study, the mentioned statistical parameters correspond to differences (mean difference and root mean squared difference) rather than errors (Bias and RMSE). Finally, in order to quantify and inter-compare sea state variability at the different sites, the area occupied by nodes presenting normalized bias and SI lower than empirically-defined thresholds were computed. This methodology is adapted from the method implemented by NENCIOLI & QUARTLY (2019), who investigated the performance of the Sentinel-3 altimetry mission for measuring waves in the coastal zone.

3. Results

3.1 Model validation

Table 2 shows the bias, RMSE and SI between model and observations for each buoy and each wave parameter. For the peak direction, which is 2π-pi periodic, circular statistics

were used to compute the bias and RMSE. Moreover, since the quality flags provided in the CMEMS INSTAC products were not sufficient to filter out every spurious measurement, an outlier detection method has been implemented based on the iteratively reweighted least squares robust regression method, which assigns a weight between 0 and 1 to each data pair during the regression iterative process. In our case, we apply the robust regression method to the in situ–model data pairs, and reject the data if the weight is lower than 0.01.

Table 2. Statistical errors computed between model and in situ data at each buoy location (a positive bias corresponds to model data larger than in situ data).

ID	Buoy	Hs			Tp			Dp	
		Bias (m)	RMSE (m)	SI (%)	Bias (s)	RMSE (s)	SI (%)	Bias (°)	RMSE (°)
0	6200001	0.04	0.31	11.15	N/A	N/A	N/A	N/A	N/A
1	62072	0.07	0.20	15.34	0.28	1.24	17.62	-2.71	49.17
2	62076	0.01	0.18	17.01	N/A	N/A	N/A	1.68	38.92
3	6200059	0.04	0.17	20.15	0.42	2.50	34.82	-3.38	24.31
4	62077	0.33	0.37	16.59	N/A	N/A	N/A	1.38	34.34
5	6200069	0.26	0.37	11.26	-0.16	1.06	9.32	4.63	13.40
6	6200074	0.07	0.25	10.72	-0.12	1.13	10.12	0.82	15.20
7	6200078	0.08	0.22	13.20	0.16	1.52	14.69	3.81	22.16
8	6200067	0.04	0.15	9.95	-0.11	1.21	10.56	N/A	N/A
9	6200080	0.04	0.21	9.62	-0.02	1.15	10.36	1.29	11.19
10	6200064	0.02	0.25	11.98	-0.18	1.11	9.68	-0.03	8.25
11	6200066	-0.04	0.30	14.62	-0.18	1.14	9.84	-0.20	8.20
	MEAN	0.08	0.25	13.47	0.01	1.34	14.11	0.73	22.51

Overall, the model shows very satisfactory performance, with average bias of 0.08 m (from -0.04 to 0.33m) for Hs, 0.01 s (from -0.18 to 0.28 s) for Tp, and 0.73° (from -3.38 to 4.63°) for Dp. The SI are 13.47%, 14.11% and 22.51% on average for Hs, Tp and Dp respectively. For Hs, we see that the model tends to slightly overestimate the observations at every site except at buoy #11 (6200066, Biarritz buoy) where the bias is negative (-0.04m). The largest bias (0.33m) is found at buoy #4 (62077, *Les Minquiers* buoy). This buoy located in the Gulf of Saint Malo is surrounded by many local shoals, which are certainly poorly resolved by the model bathymetry, which could explain why the model underestimates wave energy dissipation in this area. Largest random errors for Dp are found at buoy #1 (62072, near Boulogne-Sur-Mer), which is located near the Dover Strait, where incident waves (mostly from WSW and NNE) are strongly refracted by the Channel currents. These large errors may therefore reflect some inaccuracies in the

forcing currents. Other large Dp errors are found for buoys #2 (62076), #3 (6200059) and #4 (62077), which are all located in the Channel and affected by tidal currents. Largest random errors for Tp are found at buoy #3 (6200059, near Cherbourg), north of the Cotentin peninsula. At this location, the model regularly underestimates wind seas occurring simultaneously with NW swell events and dominating the observed energy spectrum (not shown). This could be the result of the coarse resolution of the forcing wind fields, but further investigation is needed to confirm this hypothesis. All in all, the model hindcast is able to simulate the selected bulk wave parameters with satisfactory accuracy and precision, which is particularly challenging knowing the very strong interactions between waves, winds, currents and bathymetry in the coastal regions (ARDHUIN *et al*., 2012; ALDAY *et al., 2022*).

3.2 <u>Sea state variability</u>

Figure 2 shows, for each buoy location, the normalized bias between Hs at the buoy location (black circle) and at the surrounding nodes. Regions with positive (resp. negative) values indicate that Hs at the buoy is, on average, larger (resp. lower) than Hs in this region. First of all, we see that for the offshore buoy #0 (6200001, Gascogne buoy) there is very little variability over the 100 x 100 km^2 area (normalized bias < 5%). For all the other buoys, the most striking feature is the strong Hs gradient, with larger Hs values seaward from the buoy and lower Hs values shoreward from the buoy. This general pattern is, however, strongly modulated by the presence of islands and by the geometry of the coastline. See, for instance, how Ushant island (buoy #5 (6200069)) or Belle-île island (#6 (6200074)) block the wave energy that otherwise reaches the nearby buoy. We also observe that the amplitude of the Hs gradient greatly varies from one location to another. Four buoys (#2 (62076), #3 (6200059), #7 (6200078), #8 (6200067)) show mean Hs at least 60% (and up to 150%) lower than the mean offshore Hs. These four buoys are located in relatively shallow depths (between 10.5 m and 34m, see table 1) and two of them (#2 (62076) and #3 (6200059)) are partially sheltered from the main incident wave direction, which may explain the strong attenuation of the incident energy from offshore to the buoy. If we now look at the maps of scatter index (figure 3), indicative of the non-systematic error between the buoy and the surrounding area, we see different patterns of variability, with SI generally increasing away from the buoy location, and reaching very large values (up to 50%) in sheltered regions (bays, lagoons, estuaries, lee of islands). Once again, the offshore buoy 6200001 shows very little variability with maximum SI = 6% over the 100x100km^2 area. For the five most exposed buoys (#5 (6200069), #9 (6200080), #10 (6200064), #11 (6200066)), which are deployed in depths > 50m, the SI never exceeds 20% seaward of the buoys, which indicate that the sea states measured by these buoys are quite representative from offshore conditions once the bias is corrected (see figure 2). For the other stations, the SI remains lower than 20% mostly over a restricted area (10-50km) about the buoy position, meaning that these buoys measure sea

state conditions that are only representative of the local conditions and cannot be easily extrapolated to other regions. Since the incident wave direction is a parameter of high relevance for a number of applications (longshore drift estimates, harbor operations, wave energy converter deployments), it is also of interest to characterize the coastal sea state variability in terms of peak direction.
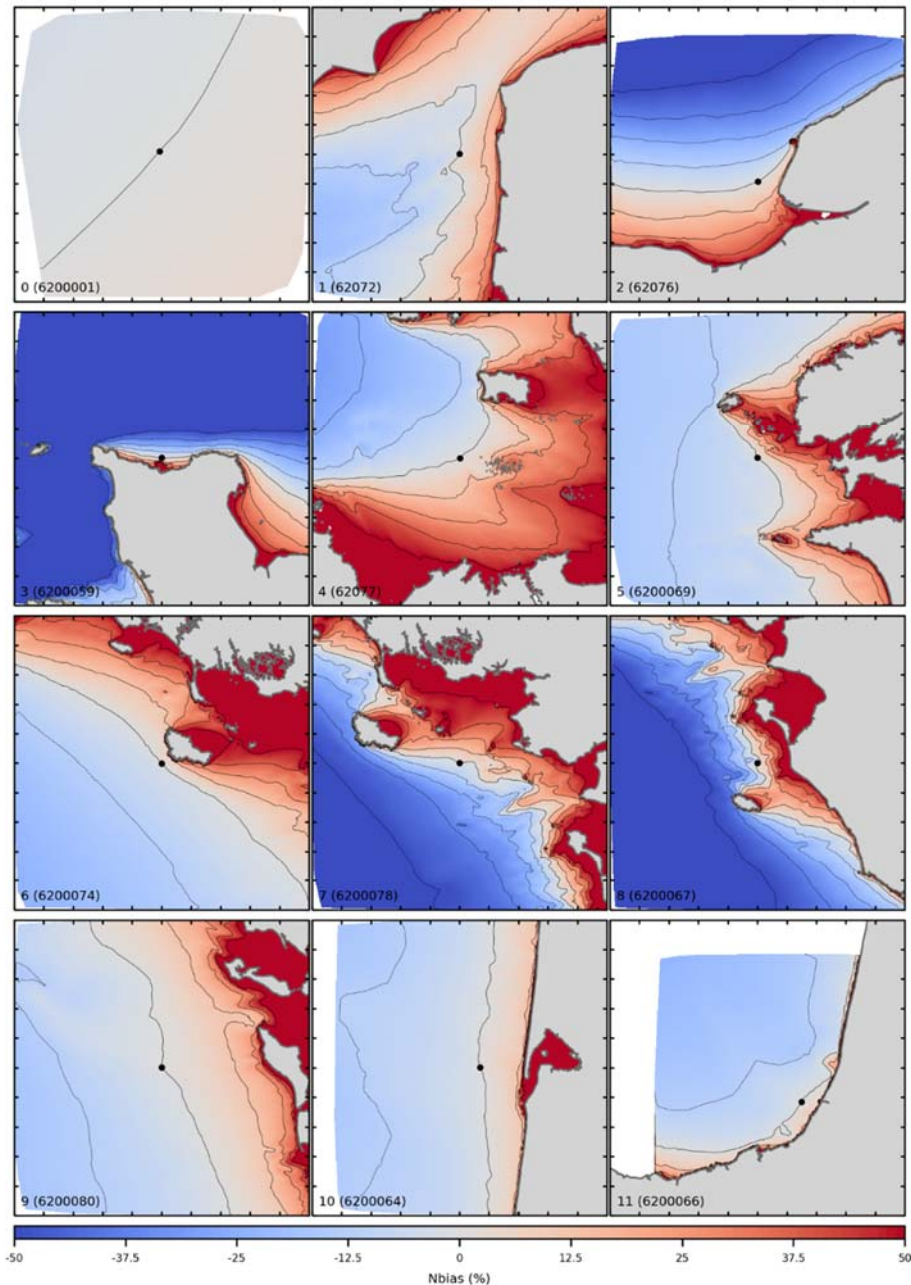
Figure 2. Maps of normalized bias (%) between Hs at the buoy location (black circles) and Hs at the surrounding nodes, for each buoy, in regions of 100x100km.
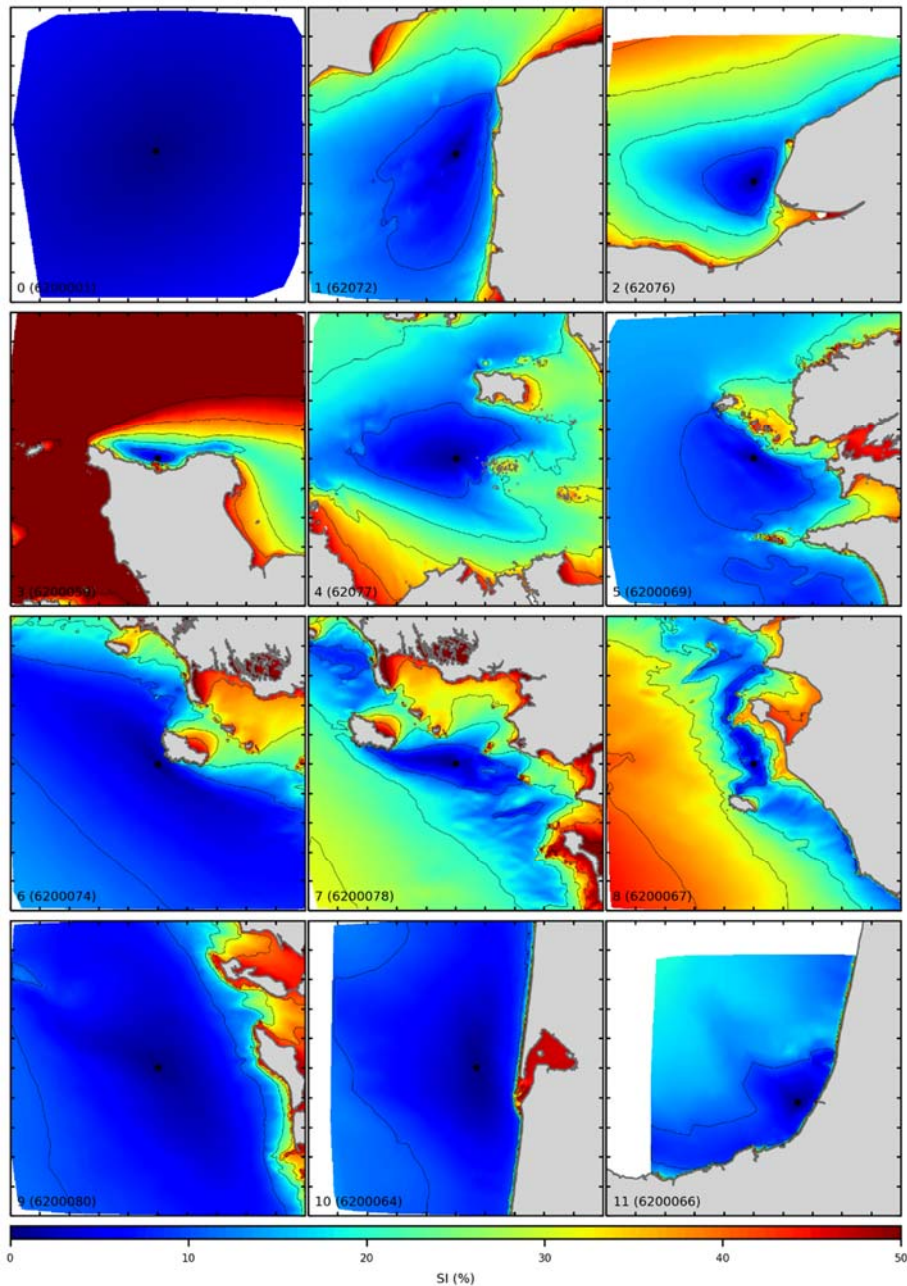
Figure 3. Maps of scatter index (%) between Hs at the buoy location (black circles) and Hs at the surrounding nodes, for each buoy, in regions of 100x100km.

Figure 4 shows the bias, RMSE and R^2 between Dp at buoy #5 (6200069) and in the surrounding area. We selected this buoy because it is the permanent station of the Iroise Sea, which is known for its strong currents, rugged bathymetry and hazardous sea state conditions. The bias map (left panel) clearly illustrates the refraction of incident swells from the North Atlantic, which bend around the Ushant island, the Molène archipelago and the *Chaussée de Sein* (a narrow submarine platform that extends the pointe du Raz).

Note that current-induced refraction is tidally modulated and does not necessarily result in systematic errors when considering all tide conditions. The RMSE map (middle panel) also shows the largest errors in the nearshore areas, where waves turn because of bathymetry refraction and where Dp bias is large. The R^2 map, however, reveals a different pattern with very low R^2 values (<0.5) NW of Brittany coastline, where tidal currents are strong and likely introduce nonlinear relationship with the peak direction at the buoy location.
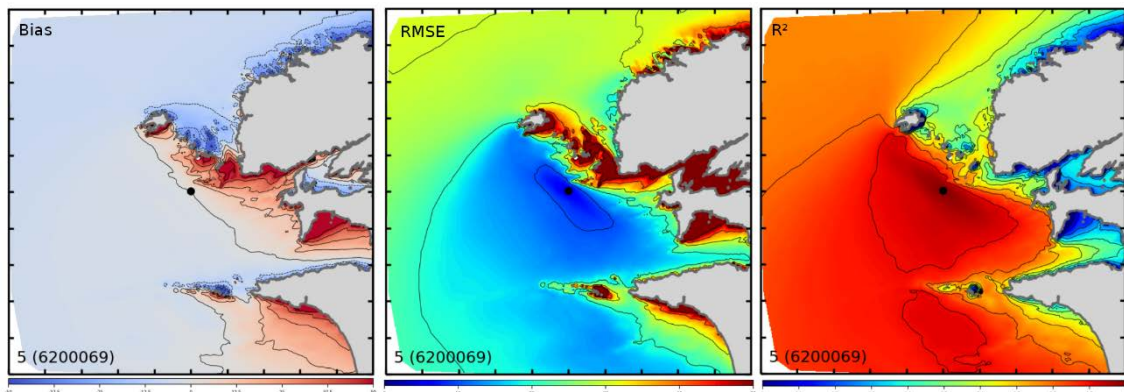
Figure 4. Maps of bias (°), RMSE (°) and R^2 between Dp at the buoy 5 (6200069) location (black circle) and Dp at the surrounding nodes.

3.3 Areas of sea state similarity

In order to quantify and inter-compare sea state variability at the different sites, we computed the surface area occupied by all the model nodes presenting low normalized bias and scatter index for Hs, Tp and Dp. The thresholds used for Hs and Tp are 5% for the normalized bias and 10% for SI, which correspond to error levels met by current state-of-the-art wave models in deep water conditions (e.g. ALDAY *et al.,* 2021). For Dp, absolute errors were used with the following thresholds: bias < 5° and RMSE < 20°. Figure 5 shows the areas of similarity for Hs and table 3 provides the associated surface area in km^2 obtained for each buoy for Hs, Tp and Dp. First of all, we can see that the area of similarity for the offshore Gascogne buoy #0 (6200001) covers the entire considered domain (~10000km^2), which means that the sea state parameter provided by this buoy can be considered homogeneous within at least a 50km radius circle, according to the selected error thresholds. If we focus on the areas of similarity for Hs (figure 5), we see that these areas are very constrained and present distinct shape and extent for each buoy, illustrating the very diverse processes that cause enhanced sea state variability in the coastal zone. In particular, buoy #3 (6200059) presents the smallest area of Hs similarity (17km^2), followed by buoys #2 (62076), #8 (6200067), #11 (6200066), #4 (62077) and #7 (6200078). For buoys #2 (62076) and #4 (62077) buoys, the areas form continuous patches around the buoy location. For buoys #7 (6200078) and #8 (6200067), the areas are on the contrary very narrow and split in several patches that follow the

bathymetric features. The buoys #6, #9, #10, #11 located in water depth > 50m also show elongated areas but much wider, showing a lower impact of wave-bathymetry interactions. Buoy #5 (6200069) is also located in water depth > 50m but it shows scattered areas of similarity due to the presence of numerous islands and strong currents in the Iroise Sea.
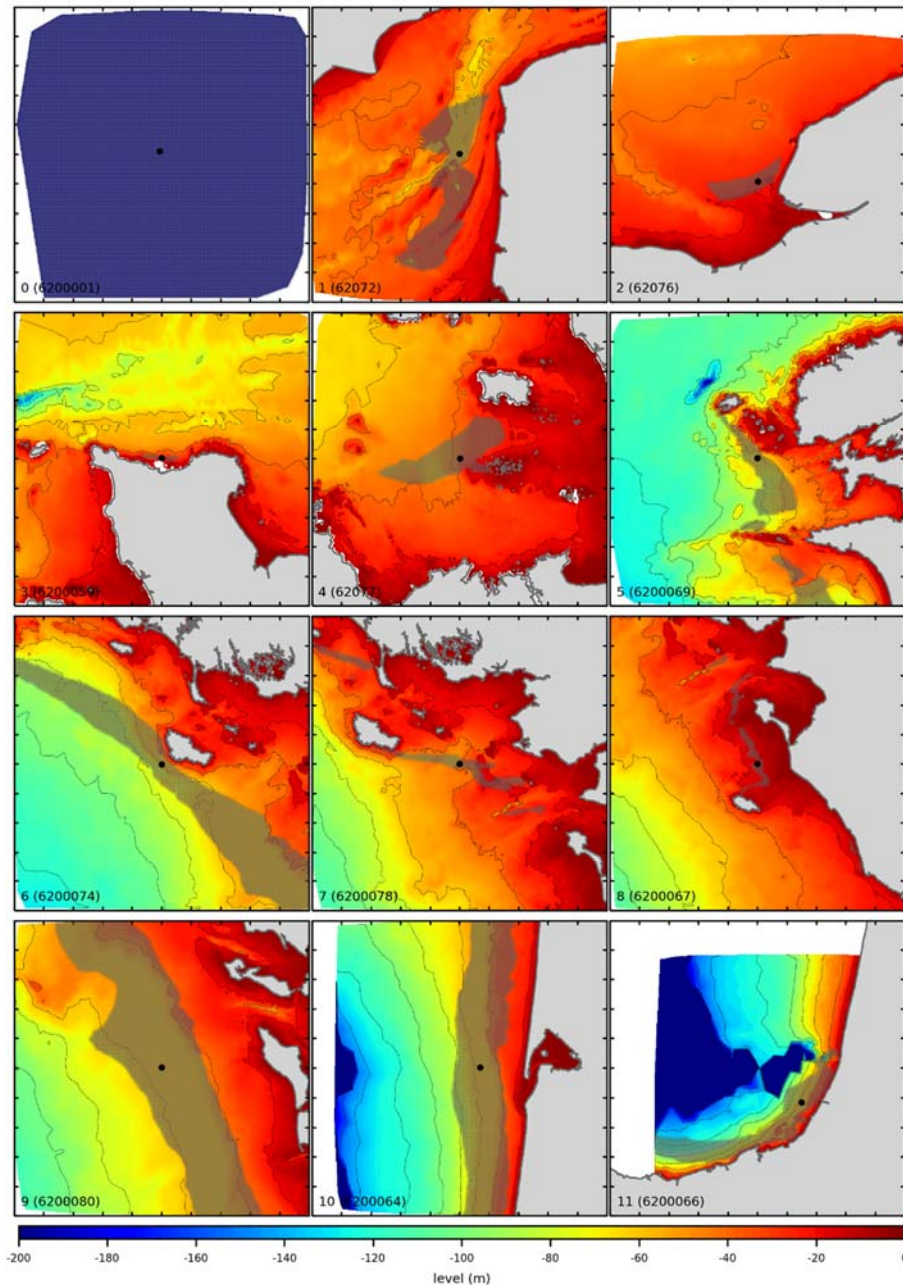
Figure 5. Bathymetric maps with areas of Hs similarity (grey area).

If we compare the area of similarity obtained for each wave parameter (table 3), we see that the relative order is usually conserved, indicating that the coastal processes affecting the wave transformation impact the entire wave energy spectrum. For similar error levels, we note that the surface areas of similarity are usually much larger for Tp than for Hs, as expected by the limited impact of bathymetric changes on the peak period. However, a few stations show very small areas of Tp similarity, which indicates large modifications of the spectral shape within small distances, probably due to current-induced Doppler shifts of Tp or sheltering of the dominant swell systems.

Table 3. Maximum surface area (km^2) surrounding each wave buoy for which the error statistics fall within the following thresholds: Hs NBIAS < 5% & Hs SI < 10%; Tp NBIAS < 5% & Tp SI < 10%; Dp BIAS < 5% & Dp RMSE < 20%.

ID	Buoy	Hs	Tp	Dp
0	6200001	8891	8891	8891
1	62072	1212	46	139
2	62076	141	51	169
3	6200059	17	1	27
4	62077	642	997	1393
5	6200069	936	5863	4421
6	6200074	1643	4255	3596
7	6200078	815	103	2000
8	6200067	591	3436	3874
9	6200080	3031	7329	6090
10	6200064	1797	6414	6063
11	6200066	624	2269	3778

4. Discussion and conclusion

Using an unstructured high-resolution numerical wave model able to resolve small-scale bathymetric and coastline features, and including the effect of tidal currents and sea level modulations on waves, we investigated the spatial variability of sea state parameters in the vicinity of coastal wave buoys along the French Atlantic coast. In comparison to the offshore buoy, we showed a very strong variability of sea state parameters, in particular Hs and Dp, for each coastal location. In particular, systematic variability patterns were put in evidence with larger Hs seaward of the buoys and lower Hs shoreward of the buoys. This coastal sea state variability can be attributed to several environmental factors, such as the presence of islands, shoals and rugged coastline, the amplified tidal currents and sea level variations over the shelf, the intermediate to shallow water condition together with the strong bathymetric gradients. It should be noted that the high variability depicted here by the model is certainly a smooth version of the reality, because of the coarse forcing fields and interpolated bathymetry soundings.

Considering this strong coastal sea state variability is important for several applications. For instance, in situ wave platforms are generally considered as the gold standard for calibrating and validating spaceborne wave measurements. Recent advances in coastal altimetry suggest that altimeter observations could be exploited as close as a few km from the coast (PASSARO *et al.,* 2021). Since satellite tracks do not necessarily pass over in situ platforms it is generally accepted to assume a homogeneous field over X kms. For offshore locations, we often consider a radius of 50-100km to be acceptable. With our result, we clearly show that more stringent criteria need to be used for comparing satellite and in situ data in the coastal zone. Moreover, recent studies proposed to evaluate the impact of waves on coastal extreme sea level at global scale (e.g. MELET *et al*. 2018). These studies generally use "coastal" outputs from coarse global hindcast to estimate the wave setup that adds up to the mean sea level and atmospheric surge at the coast. It is clear from our results that such approaches can only provide an integrated view of the incident wave energy, with a systematic tendency to overestimate nearshore wave conditions, and with high uncertainties at local scales.

5. References
ACCENSI M., ALDAY GONZALEZ M.F., MAISONDIEU C., RAILLARD N., DARBYNIAN D., OLD C., SELLAR B., THILLEUL O., PERIGNON Y., PAYNE G., O'BOYLE L., FERNANDEZ L., DIAS F., CHUMBINHO R., GUITTON G. (2021). *ResourceCODE framework: A high-resolution wave parameter dataset for the European shelf and analysis toolbox*. Presented at the EWTEC 2021 - 14th European Wave and Tidal Energy Conference, 5th to 9th September 2021, Plymouth, UK.
ALDAY M., ACCENSI M., ARDHUIN F., DODET G. (2021). *A global wave parameter database for geophysical applications. Part 3: Improved forcing and spectral resolution*. Ocean Modelling 166, 101848. https://doi.org/10.1016/j.ocemod.2021.101848
ALDAY M., ARDHUIN F., DODET G., ACCENSI M. (2022). *Accuracy of numerical wave model results: Application to the Atlantic coasts of Europe*. EGUsphere 1–39. https://doi.org/10.5194/egusphere-2022-481
ARDHUIN F., ROLAND A., DUMAS F., BENNIS A.-C., SENTCHEV A., FORGET P., WOLF J., GIRARD F., OSUNA P., BENOIT M. (2012). *Numerical wave modeling in conditions with strong currents: dissipation, refraction, and relative wind*. Journal of Physical Oceanography 42, 2101–2120. https://doi.org/10.1175/JPO-D-11-0220.1

Thème 1 – Hydrodynamique marine et côtière

HERSBACH H., BELL B., BERRISFORD P., HIRAHARA S., HORÁNYI A., MUÑOZ-SABATER J., NICOLAS J., PEUBEY C., RADU R., SCHEPERS D., SIMMONS A., SOCI C., ABDALLA S., ABELLAN X., BALSAMO G., BECHTOLD P., BIAVATI,G., BIDLOT J., BONAVITA M., CHIARA G.D., DAHLGREN P., DEE D., DIAMANTAKIS M., DRAGANI R., FLEMMING J., FORBES R., FUENTES M., GEER A., HAIMBERGER L., HEALY S., HOGAN R.J., HÓLM E., JANISKOVÁ M., KEELEY S., LALOYAUX P., LOPEZ P., LUPU C., RADNOTI G., ROSNAY P., DE ROZUM I., VAMBORG F., VILLAUME S., THÉPAUT J.-N. (2020). *The ERA5 global reanalysis*. Quarterly Journal of the Royal Meteorological Society 146, 1999–2049. https://doi.org/10.1002/qj.3803

MELET A., MEYSSIGNAC B., ALMAR R., LE COZANNET G., (2018). *Underestimated wave contribution to coastal sea-level rise*. Nature Clim Change 8, 234–239. https://doi.org/10.1038/s41558-018-0088-y

NENCIOLI F., QUARTLY G.D. (2019). Evaluation of sentinel-3a wave height observations near the coast of Southwest England, Remote Sensing, 11 (24), 2998, doi:10.3390/rs11242998

PASSARO M., HEMER M.A., QUARTLY G.D., SCHWATKE C., DETTMERING D., SEITZ F. (2021). *Global coastal attenuation of wind-waves observed with radar altimetry*. Nat Commun 12, 3812. https://doi.org/10.1038/s41467-021-23982-4

VIGNUDELLI,S., BIROL F., BENVENISTE J., FU L.-L., PICOT N., RAYNAL M., ROINARD H. (2019). *Satellite altimetry measurements of sea level in the coastal zone*. Surv Geophys 40, 1319–1349. https://doi.org/10.1007/s10712-019-09569-1